

RESEARCH ARTICLE

## Temporal and Spatial Dynamics of Inherent and Apparent Optical Properties in A Shallow Coastal Lake (Fogliano Lagoon, Circeo National Park)

Luca Bracchini<sup>1,\*</sup>, Arduino Massimo Dattilo<sup>1</sup>, Steven Arthur Loiselle<sup>1</sup>, Antonio Tognazzi<sup>1</sup>, Vincent Hull<sup>2</sup>, Claudio Rossi<sup>1</sup>

<sup>1</sup>Dipartimento Farmaco Chimico Tecnologico, Università di Siena e C.S.G.I., Via A. Moro 2, 53100, Siena, Italia.

<sup>2</sup>Laboratorio Centrale di Idrobiologia, Via del Caravaggio 107, 00147, Roma, Italia.

\*Corresponding author. Tel +39-0577-234369, Fax +39-0577-234177, e-mail address: [bracchini@unisi.it](mailto:bracchini@unisi.it)

### Abstract

- 1 - The spatial and temporal dynamics of apparent and inherent optical properties in the coastal lagoon of Fogliano were measured in three seasonal surveys in 2002. Ultraviolet and visible solar irradiance data from in situ measurements permitted to estimate the related attenuation coefficients. The extinction measurements on filtered (0.22  $\mu\text{m}$ ) and unfiltered water samples were also performed. The integrated approach between in situ and laboratory measurements allowed the determination of the role of the suspended and dissolved matter in the attenuation and extinction of ultraviolet and visible radiation within the water column.
- 2 - The impact of the suspended matter on the lake optical quality was influenced by wind resuspension of particulate matter: the relative role of dissolved matter in the absorption of UV and visible radiation was prevailing at low wind velocity conditions (less than 2.2  $\text{ms}^{-1}$ ), while at high wind velocities (3.9  $\text{ms}^{-1}$ ), particulate matter resuspension strongly influenced the attenuation and the extinction measurements. It is a surprise that the dissolved matter is not influenced by the resuspension.
- 3 - The extinction in the analyzed wavelengths of filtered and unfiltered water samples and the in situ irradiance measurements allowed us to define new optical parameters and important correlations with limnological and classical optical measurements.
- 4 - By sampling at high spatial resolution (18 stations in 4  $\text{km}^2$ ), it was possible to evidence a spatial gradient of the optical and limnological properties, these distributions showed a consistent pattern in all three surveys, and were important for the characterisation of the chromophoric dissolved organic matter that was estimated with the spectral slope of the extinction curve spectra. A relatively higher spectral slope was found in the southern basin respect to the northern, where the maximum values of the attenuation coefficients and limnological parameters were found.
- 5 - These results suggest different sources of dissolved organic matter and/or a different level of photobleaching.

**Keywords:** CDOM dynamics, UV, Absorption, Lagoon.

**Abbreviation:** IOP, Inherent Optical Properties; AOP, Apparent Optical Properties; CDOM, Chromophoric Dissolved Organic Matter; TSS, Total Suspended Solid; CHLa, Chlorophyll a; LM, Levenberg- Marquardt.

## Introduction

The spatial and temporal dynamics of the inherent optical properties (IOP) and apparent optical properties (AOP) of aquatic natural systems provide important information regarding the ecological patterns. IOPs can be investigated at the laboratory using collected water samples together with a spectrophotometric approach. The determination of the extinction coefficients of ultraviolet (100-400 nm) and visible (400-700 nm) radiation of the water samples is one of the most common measurements for this scope (Morel, 1988, Morel, 1991, Huovinen et al., 2003). AOPs can be measured in situ using spectroradiometers, the attenuation of downward spectral or band irradiance is important and often reported AOP (Kirk, 1994; Morris et al., 1995). The spectral and band attenuation coefficients ( $K_{d,\lambda}$ ,  $m^{-1}$ ) in the solar ultraviolet B (UV-B, 290-315 nm), A (UV-A, 315-400 nm) and visible (400-700 nm) wavelengths include the contribution of water itself, as well as that associated with the concentration and quality of non living particles, dissolved organic matter and phytoplankton (Kirk, 1994, Maker and Smith, 1982; Smith and Baker, 1978). The spectral extinction ( $m^{-1}$ ) of the water sample, as determined with a spectrophotometer, is also influenced by the absorption of these components as well as an increase in pathlength associated with scattering phenomena, which plays an important role in extinction measurements with respect to in situ measurements. The spectral extinction can also be used to classify water masses from an optical point of view in function of the wave form of the spectral extinction curve (Morel and Prieur, 1977; Prieur and Sathyendranath, 1981).

The linkage between attenuation coefficient (AOP), (in which e.g. the solar zenithal angle can modify the  $K_{d,\lambda}$  value), and measured extinction (IOP) was modelled

by Gordon (1989) and Kirk (1981). In most cases, the difference between the adjusted and unadjusted attenuation coefficients is reported to be negligible. In this sense, the attenuation coefficients, in particular in the ultraviolet and low wavelength of the visible spectra, were considered as quasi inherent optical properties of the medium [Baker and Smith, 1979; Zheng et al., 2002].

The spectral extinction measurements of water samples have been used to evaluate the role and the contribution of the dissolved and particulate fractions of the media to the total extinction (Kirk, 1980). Spectral extinction measurements have been utilized to examine the spatial and temporal changes of dissolved organic matter concentrations (the chromophoric portion being CDOM), total suspended solid concentrations (TSS,  $mg\ l^{-1}$ ) and chlorophyll *a* concentrations (CHL<sub>a</sub>,  $\mu g\ l^{-1}$ ) (Bracchini et al., 2004). In internal water bodies, CDOM is usually directly responsible for the natural attenuation and extinction of the UV and low wavelengths visible radiation (Scully and Lean, 1994, Laurion et al., 1997). In particular ecosystems (or periods), where (when) CDOM concentrations are low, phytoplankton and non living suspended matter assume the major role in the UV attenuation (or extinction) (Ayoub, et al., 1997; Sommaruga and Psenner, 1997; Sommaruga, 2001; Belize et al., 2002).

In internal aquatic ecosystems (as lakes) the analysis of the inherent and apparent optical properties can be represented with low uncertainty in the estimated points, using the Kriging interpolation method when spatial resolution of the sampling stations is high (Bracchini et al., 2004). This technique permits the evaluation of aquatic ecosystem patterns related to the changes in the optical properties generated by the influences of the rivers and coasts.

In the present study, the AOP and IOP

of the shallow coastal lake of Fogliano were investigated. The in situ spectral attenuation coefficients at 305, 313, 320 and 340 nm were calculated and compared with the extinction of dissolved fraction at the same wavelengths. The attenuation coefficients in the photosynthetic available radiation waveband were also computed. A comparison between the IOP for the dissolved fraction and the water column AOP (vertical attenuation) allowed to estimate the importance of suspended particles in the UV attenuation in relation of the changes in space and time. The spectrophotometric extinction measurements of unfiltered and filtered water samples allowed to estimate the role on total extinction of the suspended and dissolved particles.

The role of the particulate and dissolved fraction in attenuation and extinction was analyzed in three surveys and the spatial distribution of the optical properties in each survey was determined, which show specific spatial characteristics of the lake over time. The defined optical parameters were compared with the total suspended solid and chlorophyll a concentrations. The resuspension effect (driven by the wind) increase the suspended particles concentration in the water column as well as it amplify the importance of the suspended matter on attenuation and extinction of UV and visible irradiance. The wind resuspension appear don't increase the concentration of the dissolved particles (measured as spectrophotometric absorption). The ratio between UV attenuation coefficients and extinction of the filtered samples as well as the derived filtered and unfiltered extinction parameters are sensitive to the variations of the concentrations of the limnological properties in the lake (in space and in time) and the related role of suspend and dissolved particles on the UV and visible optical properties. The importance of the dissolved and particulate fractions

for the attenuation of UV and visible solar radiation contributes to the comprehension of the role that different spectral portions of solar radiation play on biotic and abiotic structures of aquatic ecosystems.

## Materials and Methods

### 2.1 Study site

The Pontine Lagoons are located 100 km south of the city of Rome (Italy), in the territory of the National Park of Circeo. The Lake of Fogliano (surface 4 Km<sup>2</sup>; Figure 1 a) is the largest of the three park lakes and the object of the present study. The south west part of the lake is separated from the Tyrrhenian Sea by a coastal sandy dune characterized by typical Mediterranean coastal vegetation. The north-easternmost territory, off the lake borders, is characterized by an extensive agriculture area with zootechnical activities, mainly water buffalo. A limited exchange, between the marine and lake waters, occurs through a 10 m wide canal, with the flowrate being controlled by tides. All freshwater inputs have been deviated to reduce pollutant entrainment into the lake, this has led to a strong increase in salinity (average value above 40 g l<sup>-1</sup>), in the last two decades. The average depth of the lake is around 1 m (Figure 1b). The bottom is characterized by the presence of submerged macrophytes (*Ruppia maritima* and *Cymodocea nodosa*), and a sediment consisting mainly of sandy silt. Wind direction and velocity is measured automatically at the lake border and shows typical sea breeze regimes.

Eighteen measurement sites were sampled in March, July and November of 2002 (Figure 2). The first and last survey where sampled twice on consecutive days. These repetitions were made to verify the repeatability of the measurements in relation to possible resuspension processes.

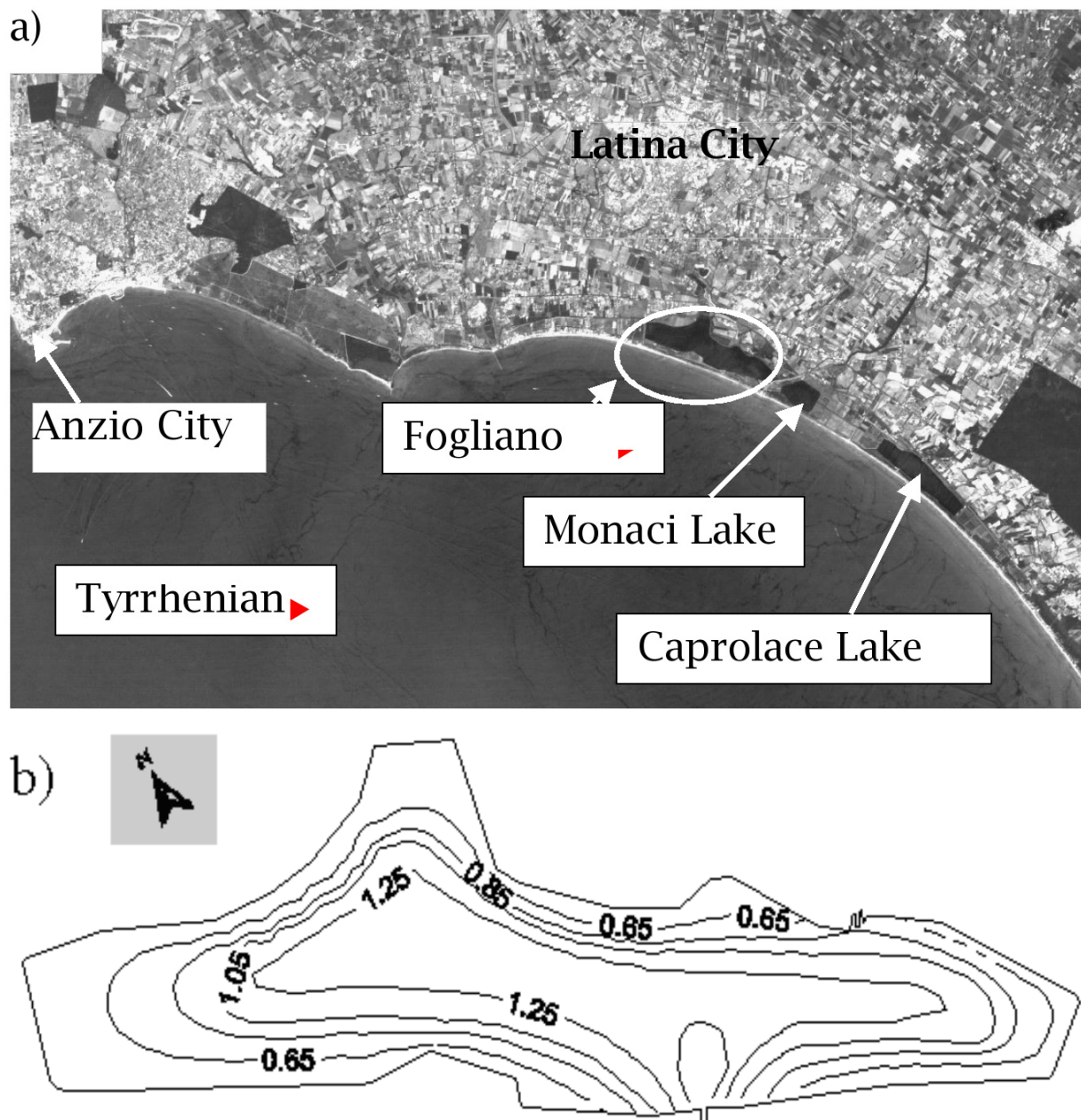


Figure 1 a: Fogliano Lake and the Circeo National Park using a georeferenced satellite image (Band 4, Landsat 7) (projection: Gauss Kruger; spheroid: WGS84; coordinate system: UTM, m). The southern side of the lake is separated from the sea by a dune ecosystem. The north part of the lake was bordered by agricultural areas. Figure 1 b: Depth contour map of Fogliano lake.

*2.2 Spectral irradiance measurements and attenuation coefficients computation*

Measurements were made between 11:00 and 15:00 (local time) in days with limited cloudiness and low wind velocity (less  $4.0 \text{ m s}^{-1}$ ). In each station, a vertical profile of the UV and Photosynthetically Available

Radiation (PAR) irradiances were measured using a PUV541 spectroradiometer SN 19235 (Biospherical Instruments, San Diego, CA). The instrument was calibrated in July 2001 comparing the measured irradiances of the instrument with a second spectroradiometer (SUV-100,

Biospherical Instruments, San Diego, CA) with a spectral resolution of 1 nm. The spectral irradiance ( $\mu\text{Wcm}^{-2}\text{nm}^{-1}$ ) channels in the UV band of the PUV541 are 305 nm (bandpass 7 nm), 313 nm (bandpass 10 nm), 320 nm (bandpass 11 nm) and 340 (bandpass 10 nm) with a cosine response. The dark current signal of the sensor, expressed in spectral irradiance units, was equal or less than  $0.001 \mu\text{Wcm}^{-2}\text{nm}^{-1}$ .

The instrument was manually lowered from the sun illuminated side of the boat (height of the boat from surface water about 0.50 m). To reduce the interferences, a staff of 2.00 m was used to increase the distance between the instrument and the boat. At the end of the staff a pulley was used to facilitate the downward and upward casting of the instrument. At each station, measurements of UV and PAR

irradiances, water temperature and water depth were acquired simultaneously every 0.3 seconds. The depth sensor was set at each sampling site to measure  $0.02 \pm 0.02$  m at the depth at which the cosine sensor of the PUV instrument was just below the surface of the water. The accuracy of the depth sensor was determined (0.02 m) by comparing the measured depth to a graduated cord, during each profile. Additionally, the depth measurement at a fixed depth did not show significant variation ( $< 0.02$  m). The irradiance measurements were recorded while the instrument was lowered to just above the lake bottom as well as during the raising of the instrument. On average, 200 measurements of irradiances, temperature ( $^{\circ}\text{C}$ ) and water depth (m) were obtained for each profile and were used to compute the attenuation coefficients. The irradiance measurements were collected between the subsurface value

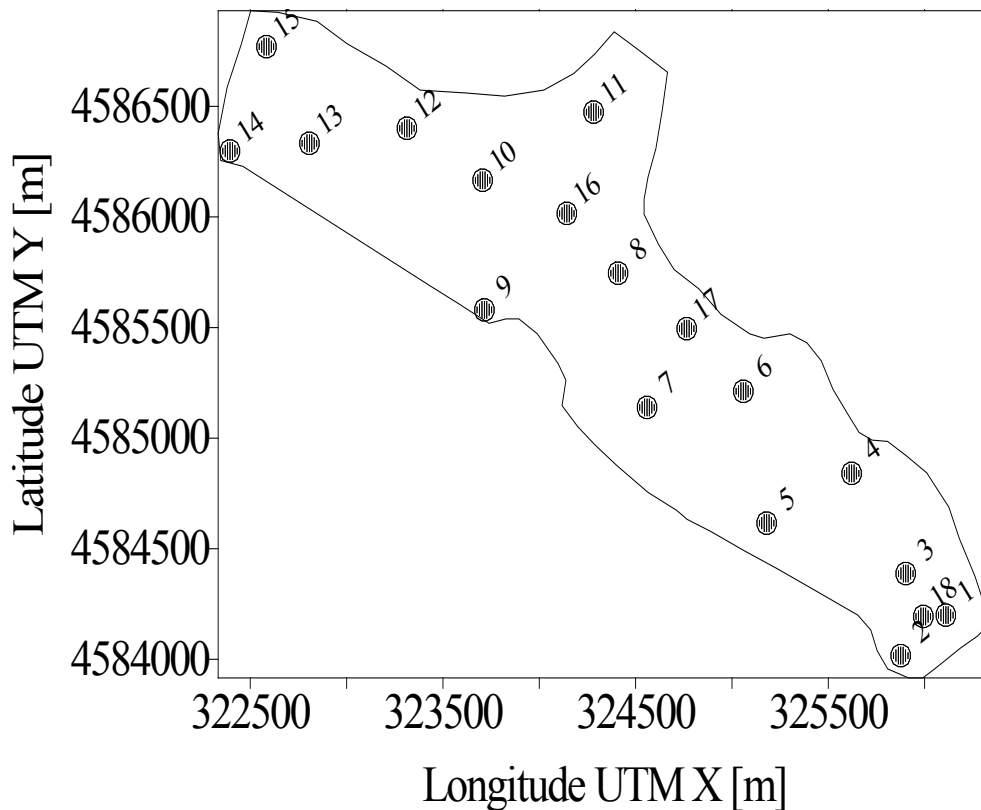


Figure 2: Spatial distribution of the sampling stations performed during the three surveys.

(0.02 m) and the maximum depth of each station. When the irradiance was measured to be below the dark current signal of the PUV, a sub interval was chosen to calculate the attenuation coefficients.

The resulting radiation profile was corrected by removing the dark current signal and plotted vs. the water depth. The attenuation coefficient was calculated by fitting the best exponential curve to the profile data for each wavelength, using Levenberg- Marquardt algorithm (LM) least square method (equation (1) hereby following).

$$I_{\lambda} = I_{0,\lambda} \text{Exp}(-K_{d,\lambda}(z - z_0)) \text{ Eq. 1}$$

Where  $z$  is water depth,  $z_0$  is 0.02 m,  $I_{0,\lambda}$  is the irradiance at 0.02 m and  $K_{d,\lambda}$  is the spectral attenuation coefficient for the downward solar radiation at  $\lambda$ . An analogous procedure was used for the PAR measurements ( $\mu\text{E m}^{-2}\text{s}^{-1}$ ) substituting the wavelength  $\lambda$  with  $\Delta\lambda = \text{PAR}$ . All profiles in which the correlation coefficient ( $R^2$ ) for Equation 1 using the measured irradiances was less than 0.97 were discarded. The graphical representation of the profiles were determined using the following modification of equation 1:

$$-\frac{K_{d,\lambda}}{2.303}(z - z_0) = \text{Log}\left(\frac{I_{\lambda}}{I_{0,\lambda}}\right) \text{ Eq. 2}$$

The boundary of the lake (Figure 2) was determined using a georeferenced satellite image (Band 4, Landsat 7) (projection: Gauss Kruger; spheroid: WGS84; coordinate system: UTM, m).

### 2.3 Extinction measurements and calculations

At each station unfiltered and 0.22  $\mu\text{m}$  filtered (Millex GP Filter Unit, Millipore S.A., Malsheim, France) water samples were

collected at 0.2 m from water surface and stored in the dark at 4°C. Spectrophotometric analyses (Cary 50, Varian, detection limit  $<0.2 \text{ m}^{-1}$ ) were performed within 24 hours, after acclimatizing of the samples to room temperature (18°C). Using a single 0.01 m quartz cuvette (Hargreaves, 2003) and distilled water (Milli-Q, Millipore) as a reference, extinction spectra were obtained from 260 nm to 700 nm with a spectral resolution of 1 nm. The speed scan was of 4500  $\text{nm min}^{-1}$ . Three complete scans of each sample were performed and the average values were calculated with the differences between the scans being close to the detection limit of the spectrophotometer. The unfiltered samples were gently agitated before each spectral scan. The high speed scan was chosen to analyze the uncertainty due to particle settling in the unfiltered sample scans. Three successive scans were performed of the unfiltered samples to examine variations in the measurements and effects related to particle settling. Eighty seconds were required to perform the three scans and twenty seconds for a single scan. No appreciable difference were observed.

The extinction spectra of the unfiltered samples is the result of both absorption and scattering characteristics of the suspended and dissolved matter present in the sample (the effect of the water itself is subtracted). The objective of these measurements was to compare the total extinction ( $e_{\lambda, \text{nf}}$ ) between samples using a laboratory spectrophotometer (with its fixed and original manufactured distance between quartz cuvette and photomultiplier). We hypothesized that the total extinction would be largely a function of the concentrations of the suspended and dissolved matter present in the lake samples. This measurement of total extinction would result in an overestimation, with respect to the determination of vertical attenuation in the water column, due to additional scattering losses which do not occur in the field. For this reason it is not

possible to quantify vertical attenuation from the spectral extinction measurements obtained in the laboratory. In both the filtered and unfiltered samples, absorption is driven by the presence of coloured dissolved matter (CDOM). Clearly, for the scattered light, the absorption caused by coloured dissolved matter is higher than in the filtered sample because of a general increase in the optical pathlength. This phenomena can not be detected by our spectrophotometer system because of the collimated detector (no integrated sphere is used). For these reasons, extinction measurements in the unfiltered samples can be considered as a overlap of absorption of CDOM in a 0.01 m optical pathlength and the scattering (and absorption) of suspended particles. From this point of view, it is possible to evaluate the extinction caused by the absorption and scattering of the suspended matter by subtracting the extinction (absorption) of the filtered sample ( $a_{\lambda,f}$ ) (driven essentially by absorption of CDOM) from the unfiltered extinction measurements (total extinction,  $e_{\lambda,nf}$ ) as:

$$e_{\lambda,nf-f} = e_{\lambda,nf} - a_{\lambda,f} \quad \text{Eq. 3}$$

where  $a_{\lambda,f}$  and  $e_{\lambda,nf}$  are absorption and extinction measurements converted in Napierian base logarithm and in  $m^{-1}$ . The two terms,  $e_{\lambda,nf}$ ,  $e_{\lambda,nf-f}$  can not be used to evaluate particle attenuation in the natural conditions but can be used to evaluate the sum of absorption and scattering in an optically collimate instrument.

Integrating the  $e_{\lambda,nf-f}$  in the visible wavelengths (400 – 700 nm), the particulate contribution to overall extinction, ( $I_{nf-f,400-700}$ ,  $m^{-1}nm$  equation 4) can be determined as:

$$I_{nf-f,400-700} = \int_{400}^{700} e_{\lambda,nf-f} d\lambda \quad \text{Eq. 4}$$

$I_{nf-f,400-700}$  was then compared to total suspended solids and chlorophyll *a* concentrations to determine the relation between of the extinction data and limnological parameters which will influence the particle extinction characteristics.

The percentage of the dissolved fraction absorption (extinction) to the unfiltered sample extinction can be computed as ( $P_{\lambda,f}$ , dimensionless; equation 5):

$$P_{\lambda,f} = \frac{a_{\lambda,f}}{a_{\lambda,nf}} = 1 - \frac{a_{\lambda,nf-f}}{a_{\lambda,nf}} = 1 - P_{\lambda,nf-f} \Rightarrow P_{\lambda,nf-f} = 1 - P_{\lambda,f} \quad \text{Eq. 5}$$

$P_{\lambda,f}$  approaches unity when the absorption of CDOM dominates the total extinction (absorption and scattering) of the suspended and dissolved matter. On the contrary the  $P_{\lambda,f}$  is near zero when the absorption and scattering related to the presence of particles is greater than the absorption due to CDOM. Both  $P_{\lambda,f}$  as well as  $P_{\lambda,nf-f}$  are wavelength dependant. Therefore these ratios can be represented as curves. When a relative high concentration of suspended particles is present in the unfiltered sample with respect to the dissolved fraction, the  $P_{\lambda,nf-f}$  curve is higher than the  $P_{\lambda,f}$  curve. The opposite would occur when high concentrations of CDOM are present. The spatial or temporal evolution of the  $P_{\lambda,nf-f}$  curves would represent the spatial and temporal variation of the role of dissolved and particulate fractions in spectrophotometric extinction.

In the filtered water sample, the spectral extinction has often been used to estimate changes in the molecular structure of the dissolved matter. We used the slope of the exponential decrease in absorption with increasing wavelength following the approach proposed by Bricaud et al. (1981) and introducing a background parameter ( $\gamma$ ,  $m^{-1}$ ) according to the following equation (6) (Markager and Vincent, 2000; Stedmon and Markager, 2000):

$$a(\lambda)_f = a(\lambda_0)_f e^{s(\lambda-\lambda_0)} + \gamma \text{ Eq. 6}$$

where,  $260 \text{ nm} \leq \lambda \leq 700 \text{ nm}$ ,  $\lambda_0 = 290 \text{ nm}$ ,  $a(\lambda_0)_f$  is the measured absorption at 290 nm and  $s$  ( $<0, \text{ nm}^{-1}$ ) is the slope of the spectra. Separating the vertical attenuation coefficient (equation 1) in parts to include both the dissolved and particle fractions;

$$K_{d,\lambda} = \frac{a_{\lambda,f}}{\mu_\lambda} + K_{d,particles} + K_{d,water} \text{ Eq. 7}$$

where  $K_{d,particles}$  the attenuation coefficient for the suspended particles,  $K_{d,water}$  the attenuation coefficient of the pure water,  $a_{\lambda,f}$  the extinction (absorption) of the CDOM and  $\mu_\lambda$  the spectral light diffuseness factor. If the attenuation coefficients for the pure water can be neglected, the ratio ( $R_\lambda$ ):

$$R_\lambda = \frac{K_{d,\lambda}}{a_{\lambda,f}} = \frac{1}{\mu_\lambda} + \frac{K_{d,particles}}{a_{\lambda,f}} \text{ Eq. 8}$$

represents the percentage of the attenuation coefficient not explained by the direct irradiance absorbed by CDOM. This ratio is composed by the sum of two terms: the first is the inverse of the diffuseness factor and the second is the ratio between attenuation due to particles and the direct beam absorbed by CDOM. Following this equation, an increase in the concentration of suspended particles should lead to an increase in the ratio  $R_\lambda$ . An increase in the concentration of CDOM should lead to a decrease in the ratio (Kirk, 1994).

#### 2.4 Limnological measurements

Water samples were analyzed to determine the concentrations of suspended matter, measured as total suspended solids (TSS), its organic and inorganic fractions and the concentration of chlorophyll *a* (CHLa) and pheopigments. TSS and the organic and inorganic particulate fractions, were measured by gravimetric methods, after in situ filtration of 1 l samples using heat treated (530°C, 5 h) pre-weighted

glass fiber filters (Millipore) (Standard methods, 1998). The filters were stored in a dry environment until the second weighting. Chlorophyll *a* and pheopigments were measured spectrophotometrically according to Strickland and Parsons (Strickland and Parson, 1972), after in situ water filtration of 0.5 l. All measurements (weightings and pigment analyses) were performed before 24 hours after sample collections.

#### 2.5 Spatial representation

To analyze the spatial distribution of optical measurements, several maps were created with the Surfer 7.0 software package using the Kriging interpolation technique. Likewise, maps of the standard deviations were also setup, but are not presented here. The values of standard deviations were used to determine the number of classes for the spatial representation maps of the optical measurements. The class interval was chosen to be equal to, or greater than, the maximum standard deviation.

## Results and discussion

The results and related discussion has been organized in the following order:

1. analysis of the temporal variation of limnological and optical measurements;
2. analysis of  $R_\lambda$  changes;
3. extinction analysis;
4. the spatial distribution of optical and limnological parameters.

#### 3.1 Analysis of the temporal variation of limnological and optical measurements

The measured irradiance profile (Eq. 2) at a single station (station 8) over the three surveys shows the variation encountered (figure 3,4,5). The maximum depth at this station reached by PUV instrument was about 0.70 m and the bottom was at 1.20 m. In the first survey the UV irradiance ratio was computable with good accuracy until 0.65 m. The PAR irradiance ratio was 0.7 at 0.70m.

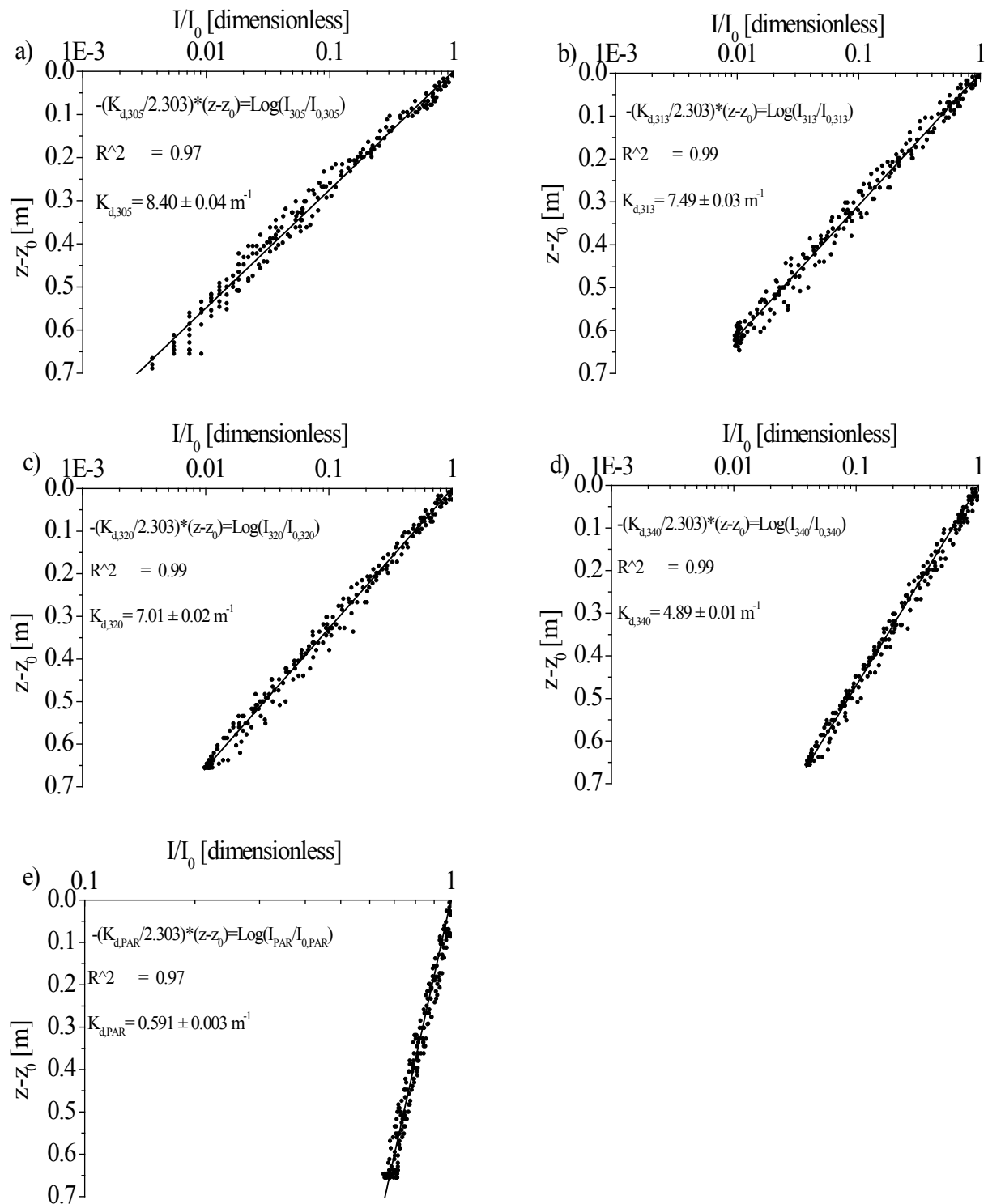


Figure 3: Measured profile ratio for 305 (panel a), 313 (panel b), 320 (panel c) and 340 nm (panel d) and PAR (panel e) irradiance at the station 8 during the first survey. In each graph, the attenuation coefficient and the square correlation coefficient are shown.

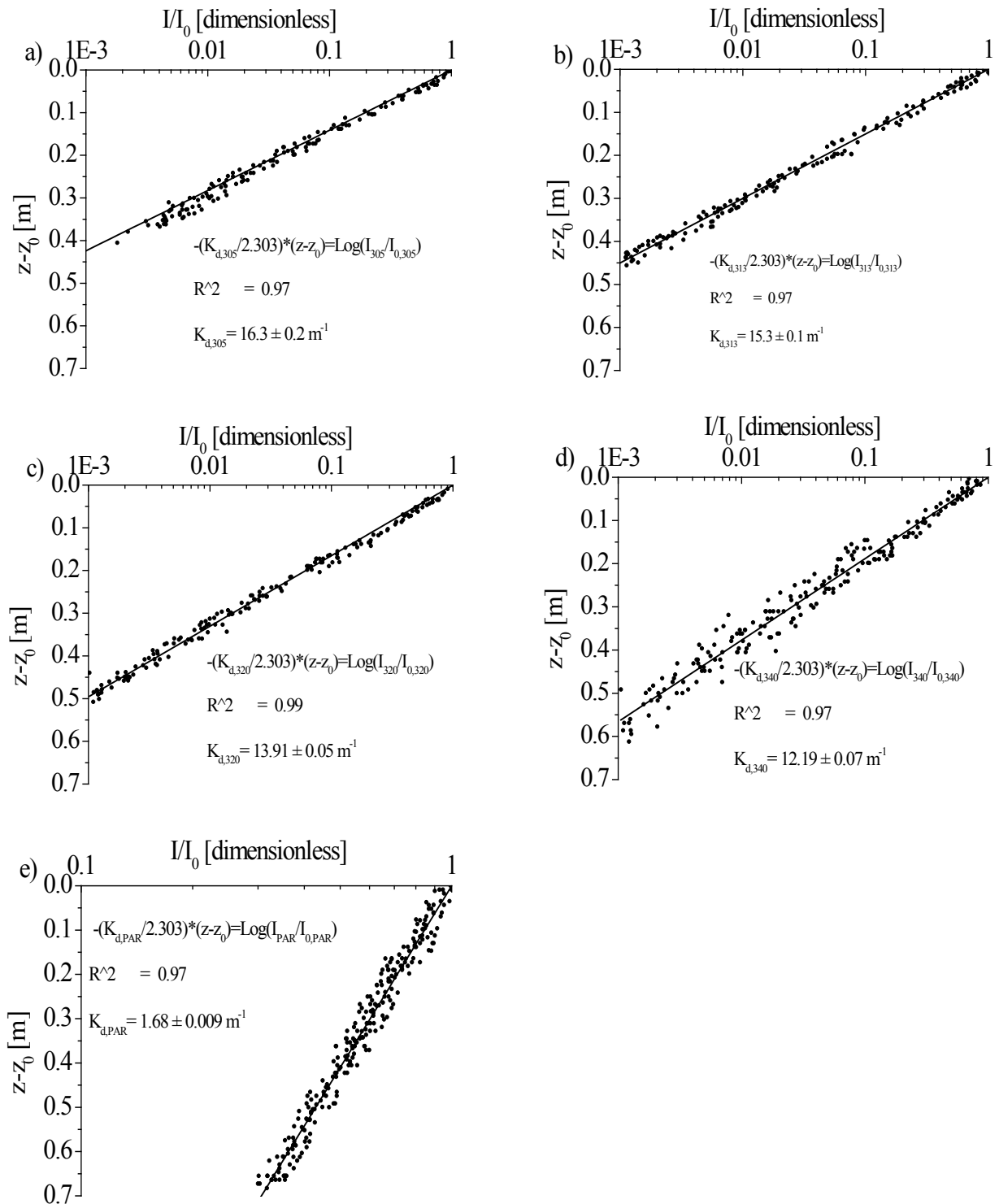


Figure 4: Measured profile ratio for 305 (panel a), 313 (panel b), 320 (panel c) and 340 nm (panel d) and PAR (panel e) irradiance at the station 8 during the second survey. In each graph, the attenuation coefficient and the square correlation coefficient are shown.

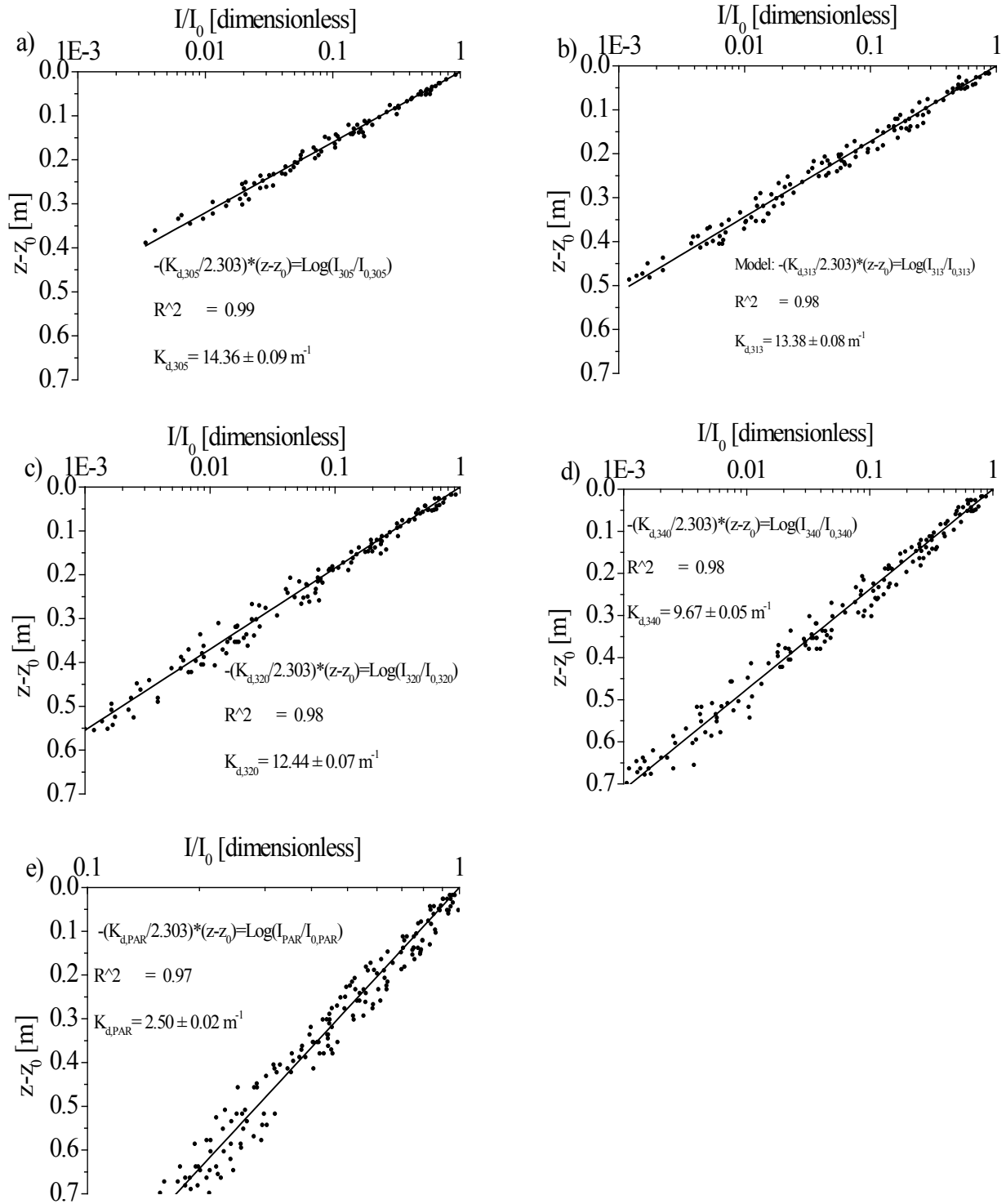


Figure 5: Measured profile ratio for 305 (panel a), 313 (panel b), 320 (panel c) and 340 nm (panel d) and PAR (panel e) irradiance at the station 8 during the third survey. In each graph, the attenuation coefficient and the square correlation coefficient are shown.

Extrapolating the measured attenuation coefficient to the bottom was gives a PAR ratio of 0.5. In the second survey (Fig 4), the UV and PAR attenuation coefficients were higher than the first survey. The 305 nm irradiance ratio is observed until 0.40 m and at 313 nm is observed until 0.45 m. The 320 nm irradiance ratio is observed until 0.50 m and at 340 nm was observed until 0.60 m. The PAR irradiance ratio was 0.3 at 0.70 m and the calculated value for the bottom was 0.1. In the third survey (Fig. 5), the UV attenuation coefficients were comparable (but lower) with the attenuation coefficients measured during the second survey. The depth in which it was possible to measure the 305 irradiance ratio was 0.40 m. At 313 nm was 0.50 m and it was 0.55 m for the 320 nm irradiance. The 340 nm irradiance ratio was measurable until the 0.70 m. The attenuation coefficient for the PAR irradiance was maximal in this survey ( $2.50 \pm 0.02 \text{ m}^{-1}$  respect  $0.591 \pm 0.003 \text{ m}^{-1}$  and  $1.68 \pm 0.01 \text{ m}^{-1}$  for the first and second surveys). The high attenuation coefficient led to the low value of the calculated irradiance ratio at the bottom: 0.05.

From these local measurements, it appears that less than 0.1% of the incident UV irradiance ratio (< 340 nm) reached the bottom. On the contrary, PAR easily reached the bottom, as the lake is quite shallow and there is a significant presence of the macrophytes develop on the bottom of the lake.

The concentrations of CHLa and TSS measured during the three surveys were positively related (figure 6 a). The maximum concentration values of these parameters were measured during the autumn survey, when CHLa concentrations reached values of  $27 \pm 5 \mu\text{g l}^{-1}$  on the first day, and  $24 \pm 3 \mu\text{g l}^{-1}$  on the second. TSS concentrations were  $71 \pm 7 \text{ mg l}^{-1}$  in the first day and  $62 \pm 9 \text{ mg l}^{-1}$ , in the second.

During the spring survey the pheopigments concentrations were  $0.3 \pm 0.2 \mu\text{g l}^{-1}$  in the first day of measurements and  $0.1 \pm 0.1 \mu\text{g l}^{-1}$

during the second., the concentrations of the inorganic fraction of TSS were  $13 \pm 2 \text{ mg l}^{-1}$  and  $14 \pm 2 \text{ mg l}^{-1}$  and the concentrations of the organic fraction of TSS were  $3 \pm 1 \text{ mg l}^{-1}$  and  $4 \pm 1 \text{ mg l}^{-1}$ . During the summer survey, the concentration of pheopigments was  $0.9 \pm 0.4 \mu\text{g l}^{-1}$ , the concentration of inorganic fraction of TSS was  $12 \pm 2 \text{ mg l}^{-1}$  and for the organic fraction it was  $5 \pm 2 \text{ mg l}^{-1}$ . In the autumn survey pheopigments concentration were  $10 \pm 4 \mu\text{g l}^{-1}$  and  $8 \pm 2 \mu\text{g l}^{-1}$  in the first and second day respectively, the concentrations of inorganic fraction of the of TSS were  $49 \pm 6 \text{ mg l}^{-1}$  and  $42 \pm 7 \text{ mg l}^{-1}$  for the two days of measurements and the concentrations of the organic fraction of TSS were measured  $22 \pm 2 \text{ mg l}^{-1}$  and  $20 \pm 2 \text{ mg l}^{-1}$ .

The average wind velocity, measured during two days before and during each survey, was  $2.2 \text{ ms}^{-1}$ ,  $1.6 \text{ ms}^{-1}$  and  $3.9 \text{ ms}^{-1}$  respectively for the three surveys. This variation in wind velocity may help explain the maximum of TSS (both fractions), CHLa (and pheopigments) concentrations in the autumn (third survey) caused by sediment resuspension. The temporal variation of the PAR average attenuation coefficient values (figure 6, b, bold line) were found to generally follow those of the average values of the CHLa (positive linear relationship:  $R^2=0.70$ ,  $p<0.05$ ) and TSS (positive linear relationship:  $R^2=0.78$   $p<0.05$ ). Maximum values of the  $K_{d,PAR}$  were measured in November. The higher value of  $K_{d,PAR}$  measured during the second survey could not be explained by the small increase in the CHLa and TSS concentrations. The attenuation coefficients in the solar UV radiation (figure 6, b small lines) were maximum in the second survey, with a minimum during the first. The average extinction of filtered samples was maximum in the second survey and no effect of wind was detected for the extinction of dissolved matter during the third survey in which the average values of extinction were found similar to the first survey (figure 6, c). The

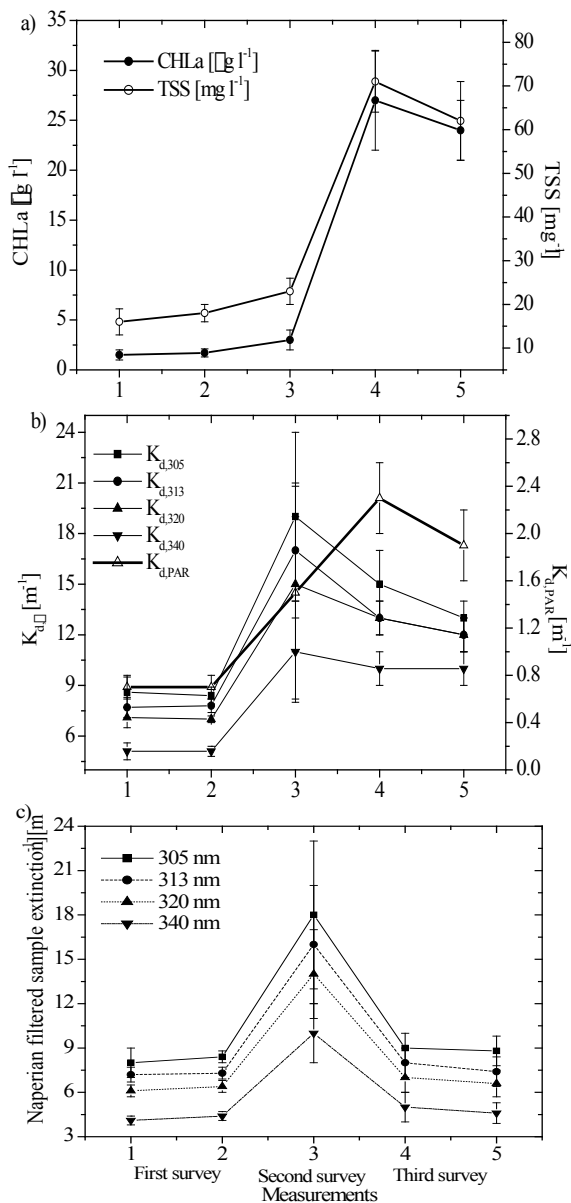


Figure 6 a: Average concentrations of total suspend solid (TSS; dark circle) and chlorophyll a (CHLa; open circle) measured during the first survey (two days of measurements), second survey (single day of measurements) and third survey (two days of measurements). Figure 6 b: Average spectral attenuation coefficients in the UV (305, 313, 320 and 340 nm; left axis, close symbols) and PAR (right axis, bold line, open symbol). Figure 6 c: Average Naperian extinction measurements of filtered (0.22  $\mu\text{m}$ ) water samples (against Milli-Q water) at 305, 313, 320 and 340 nm. All errors were calculated using the standard deviation (SD) on station measurements which also includes spatial variation.

increased value of  $K_{d,PAR}$  measured during the second survey appears to be related to increases in the dissolved fraction. The average values of UV attenuation coefficients are influenced by concentration of coloured dissolved organic matter (maximal values in the second survey) and by concentration of the TSS in the third survey.

### 3.2 Analysis of $R_\lambda$ changes

A linear relation between all calculated attenuation coefficients at 305, 313, 320 and 340 nm ( $K_{d,\lambda}$ , equation 1) and the related base 10 logarithm absorbance measurements from all surveys was found. The angular coefficients were  $221 \pm 12 \text{ m}^{-1}\text{cm}$  ( $R^2=0.82$   $N=86$ ),  $239 \pm 8 \text{ m}^{-1}\text{cm}$  ( $R^2=0.95$   $N=88$ ),  $239 \pm 7 \text{ m}^{-1}\text{cm}$  ( $R^2=0.96$   $N=88$ ) and  $256 \pm 13 \text{ m}^{-1}\text{cm}$  ( $R^2=0.88$   $N=90$ ) for 305, 313, 320 and 340 nm respectively. This further demonstrates that the UV attenuation coefficients in natural waters are primarily driven by CDOM absorption.

The independent fluctuations of concentrations of CDOM and TSS are responsible of fluctuations of  $a_{\lambda,f}$  and  $R_\lambda$ . In figure 7 Naperian spectral absorptions and  $R_\lambda$  ratios are shown for all stations in the three surveys. Similar values of  $R_\lambda$  (between 1-1.5) are observed during the first and second survey (figure 7 panel a and b). The high role of CDOM in the attenuation of UV irradiance was similar in the first and second survey. The second survey was also characterized by maximal values of the  $K_{d,\lambda}$  and  $a_{\lambda,f}$  (note the differences in the ordinate scales). During the last survey, when TSS has reached a maximum, the  $R_\lambda$  ratio has values between 1.2-2.7 (figure 7 c). The CDOM absorption was similar in the first and last survey but was more dominant in the first survey in the attenuation of UV. During the last survey, the increased values of  $R_\lambda$ , demonstrate the major role of TSS (scattering and absorption). This is a clear demonstration that the role in solar UV

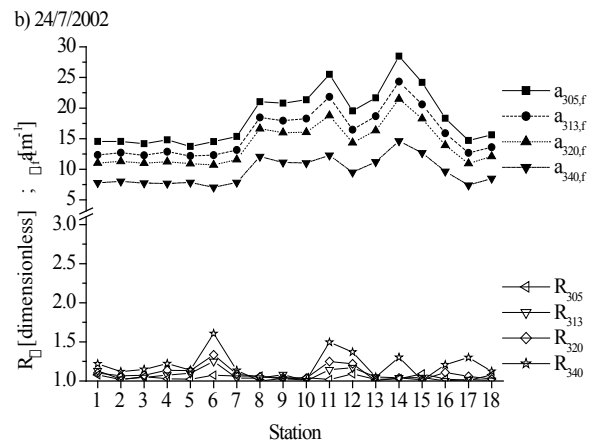
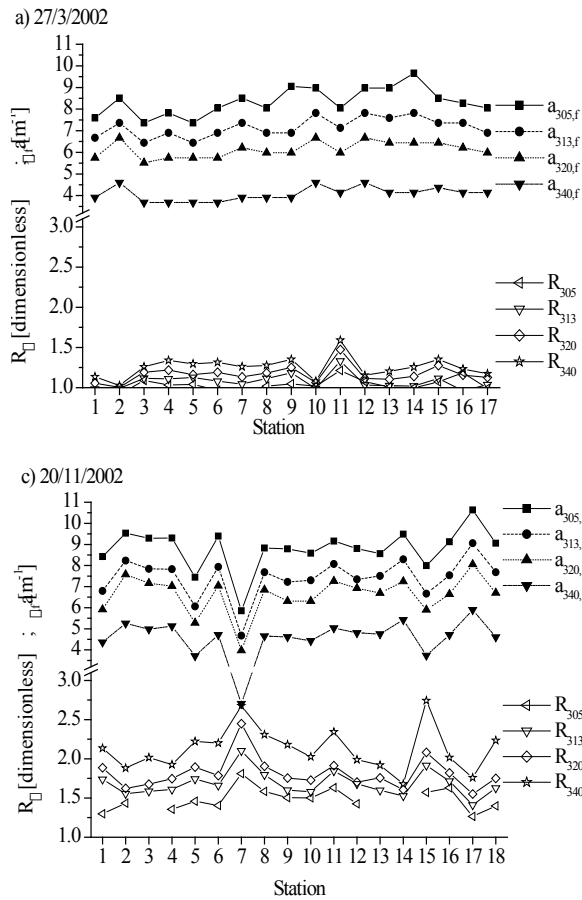


Figure 7: Naperian extinction values of the filtered water sample ( $a_{\lambda,f}$ , close symbols) collected at each station and calculated ratio ( $R_{\lambda}$ ; open symbols; equation 7) between attenuation coefficients and  $a_{\lambda,f}$  for each considered wavelength. In panel a the data of first survey are presented (27/3/2002); in panel b the data for the second survey are presented (24/7/2002) and in panel c data from third survey are showed (20/11/2002).

attenuation must be investigated according “relative concentrations” between dissolved and suspended matter. Suspended particles, and in particular phytoplankton therefore play an important role in the attenuation of UV, pointing out the importance of resuspension in the optical quality in shallow lakes.

The variations of  $R_{\lambda}$  average values (Figure 8) closely follow the changes in the concentrations of TSS and CHLa. The average  $R_{\lambda}$  values better describe the TSS temporal variation with respect the  $K_{d,PAR}$  (influenced by increasing CDOM absorption/concentration). The best positive linear relationship between  $R_{\lambda}$  are founded for the wavelength at 313 nm. This relationship is characterized by  $R^2=0.98$  and  $p<0.002$  ( $N=5$ , each point is the average of 18 measurements). The poorest relationship is observed for the  $R_{305}$  ( $R^2=0.94$  and  $p<0.005$ ).

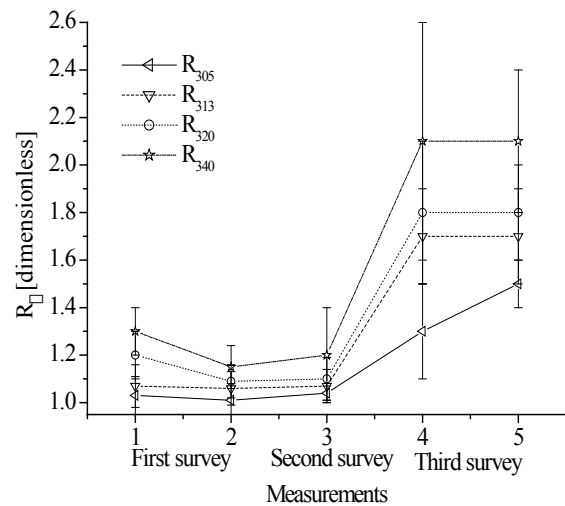


Figure 8: Average value of  $R_{\lambda}$  ratios (equation 7) calculated during the three survey for each considered wavelength (305, 313, 320 and 340 nm). All errors were calculated using the standard deviation (SD) on station measurements which also includes spatial variation.

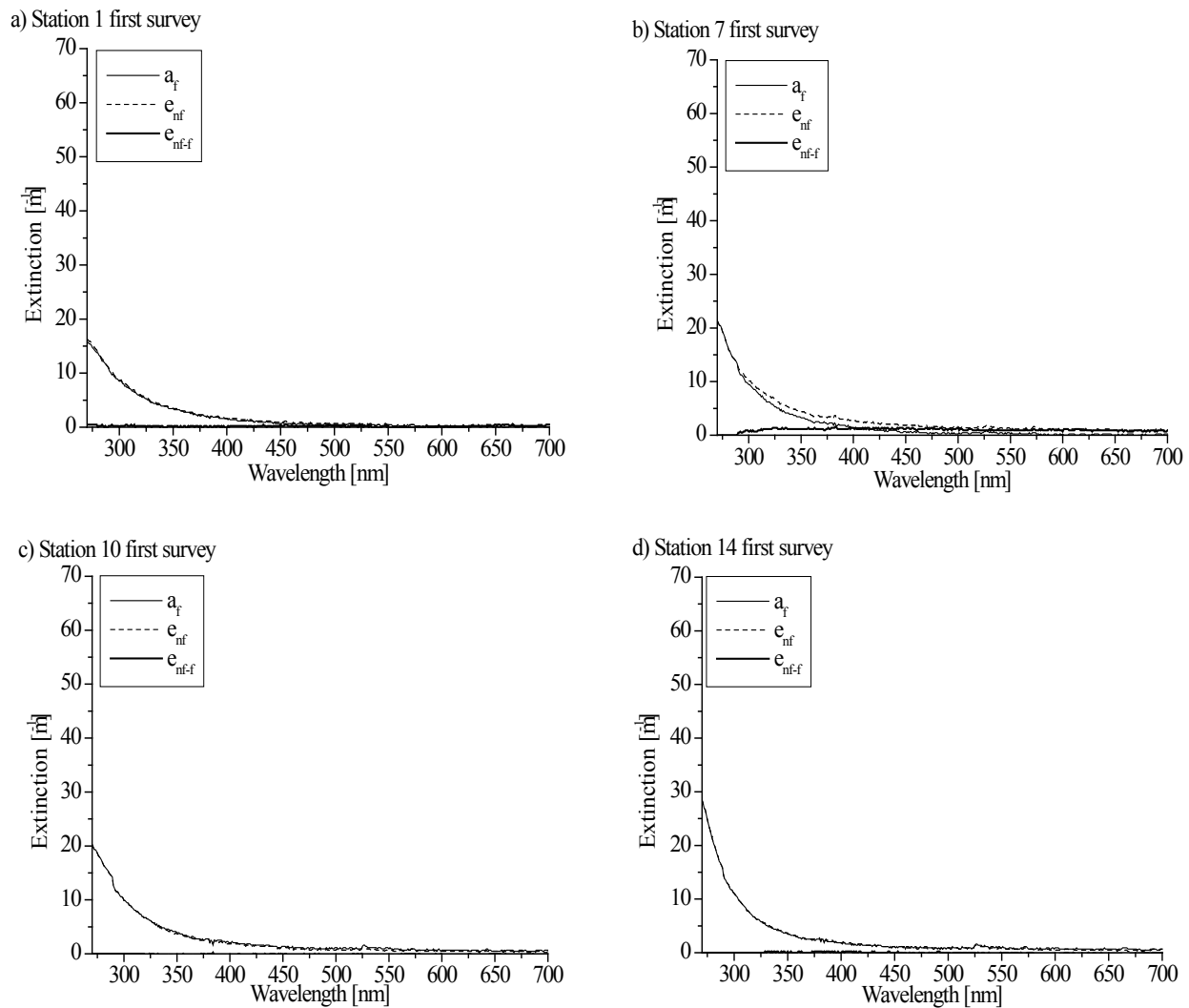


Figure 9: Spectral extinction curves, between 260-700 nm, of the filtered (0.22  $\mu\text{m}$ ) sample ( $a_f$ , solid curve), unfiltered sample ( $e_{nf}$ , dash curve) and related suspended particle calculated extinction ( $e_{nf-f} = e_{nf} - a_f$ , black bold curve). Data from first survey (station 1 panel a, 7 panel b, 10 panel c and station 14 panel d). The  $e_{nf-f}$  curves were only partially detectable during the first survey.

### 3.3 Extinction analysis

In the second survey, the average value of  $I_{nf-f,400-700}$  (equation 4) was  $2000 \pm 1000 \text{ m}^{-1}\text{nm}$ . During the third survey  $I_{nf-f,400-700}$  average values were  $2900 \pm 400 \text{ m}^{-1}\text{nm}$  on the first day and  $3400 \pm 500 \text{ m}^{-1}\text{nm}$  on the second day. The average values measured during the last survey were found to be related to the high concentrations of the TSS and CHLa.

All errors presented were calculated using the standard deviation (SD) of the measured parameter for each station. In this case the SD represents the fluctuation of the measurements but also the observed spatial

variation.

During the spring survey, the role of the particulate fraction on total extinction was negligible or undetectable in the UV and visible wavelengths (Figure 9). The total extinction ( $e_{nf,\lambda}$ , dash line) closely follows the dissolved fraction extinction ( $a_{f,\lambda}$ , black line).  $P_\lambda$  curves were omitted.

In the summer survey, the highest spectral extinction values for filtered and unfiltered samples were observed. This was driven by high concentration of the CDOM. The role of the suspended fraction was small but clearly detectable (figure 10, stations

1,7,10 and 14). This is more evident in the  $P_{\lambda,f}$  and  $P_{\lambda,nf-f}$  curves (figure 12; stations 1,7,10 and 14). The intersection (where  $P_{\lambda,f} = P_{\lambda,nf-f} = 0.5$ ) occurs at different wavelengths as a result of the dominating extinction component. The intersection at the first station samples occurred at 443 nm (figure 12, a), while at stations 7 and 14, it occurred after 600 nm (figure 12, b and d). No intersection was found at station 10 (figure 12 c). In the summer survey, extinction by the dissolved fraction dominated most of the visible spectrum, especially for the wavelengths useful for the photosynthetic activities. These results, obtained

in a collimated instrument (scattering of suspended particles is greater than in natural conditions) support the hypothesis that  $K_{d,PAR}$  is influenced by dissolved fraction absorption. High noise levels in the  $P_{\lambda}$  curves after 500 nm is the result of the small extinction values, close to the spectrophotometer detection limit. In the last survey, the high influence of TSS concentration is clearly detected (figure 11). Furthermore, it is possible to observe the in vivo extinction peak of phytoplankton around 680-690 nm in the  $e_{nf,\lambda}$  and  $e_{nf-f}$  curves (Figure 12). The related  $P_{\lambda}$  curves (figure 13) showed  $P_{\lambda,nf-f} > P_{\lambda,f}$  for each considered wavelength.

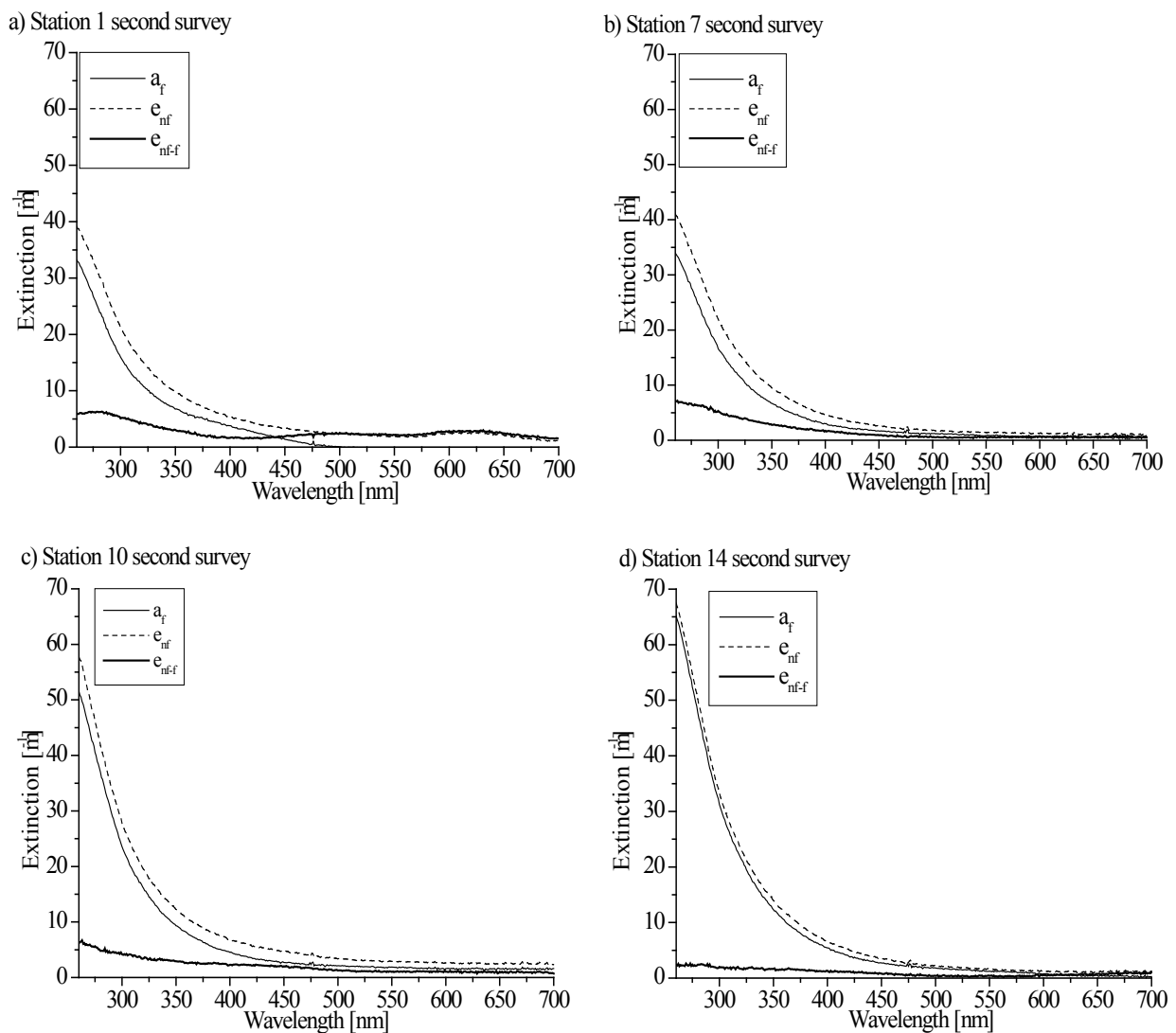


Figure 10: Spectral extinction curves, between 260-700 nm, of the filtered (0.22  $\mu$ m) sample ( $a_f$ , solid curve), unfiltered sample ( $e_{nf}$ , dash curve) and related suspended particle calculated extinction ( $e_{nf-f} = e_{nf} - a_f$ , black bold curve). Data from second survey (station 1 panel a, 7 panel b, 10 panel c and station 14 panel d).

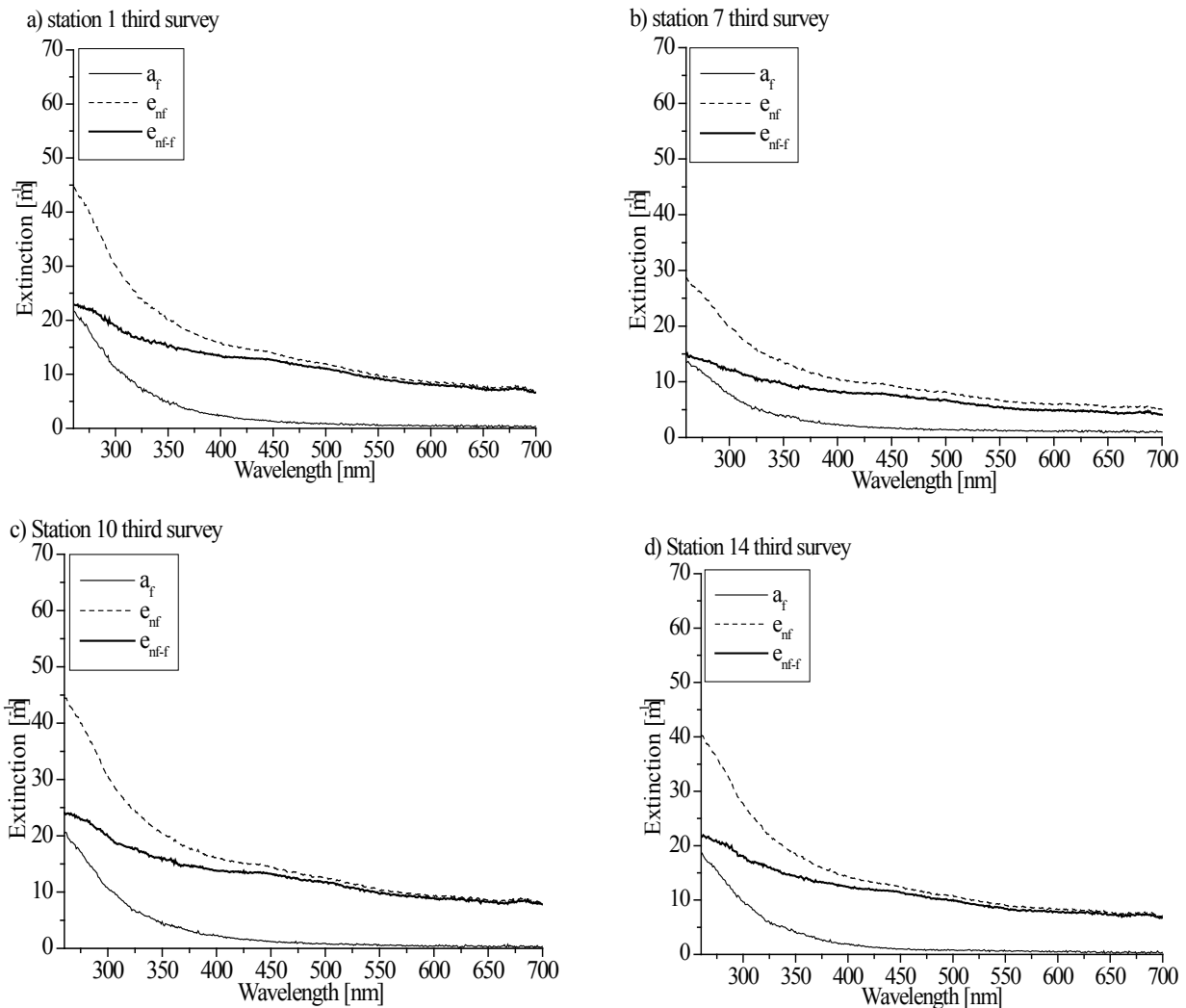


Figure 11: Spectral extinction curves, between 260-700 nm, of the filtered (0.22  $\mu\text{m}$ ) sample ( $a_f$ , solid curve), unfiltered sample ( $e_{nf}$ , dash curve) and related suspended particle calculated extinction ( $e_{nf-f} = e_{nf} - a_f$ , black bold curve). Data from third survey (station 1 panel a, 7 panel b, 10 panel c and station 14 panel d).

The  $a_{nf-f,\lambda}$  curves combine extinction due to both scattering and absorption of the particles larger than 0.22  $\mu\text{m}$ , which include most of the phytoplankton populations. The scattering process is presumable dominated by Mie scattering. This is further confirmed by its poor wavelength dependency with respect to non particle scattering (Morel, 1991; Mobley, 1994; Blumthaler and Webb, 2003). The possibility to utilise the  $e_{nf-f,\lambda}$  curve for phytoplankton estimations and for considerations about the dimension of the suspended particles (according the Angstrom formula (Shifrin, 1995)) justifies further investigation.

The average spectral slope for each survey was determined to be  $-0.022 \pm 0.003 \text{ nm}^{-1}$ ,  $-0.017 \pm 0.001 \text{ nm}^{-1}$ ,  $-0.016 \pm 0.002 \text{ nm}^{-1}$ , leading to the idea that CDOM was less able to absorb ultraviolet and visible radiation in the first survey. This suggests different levels of degradation, or a different origin of the CDOM pool, of particles in this survey in respect to the others. Differences in the spectral slope have been linked with variations in the average molecular weight of CDOM (De Haan and De Boer, 1987; De Haan, 1993), indicating a lower average CDOM molecular weight in the first survey.

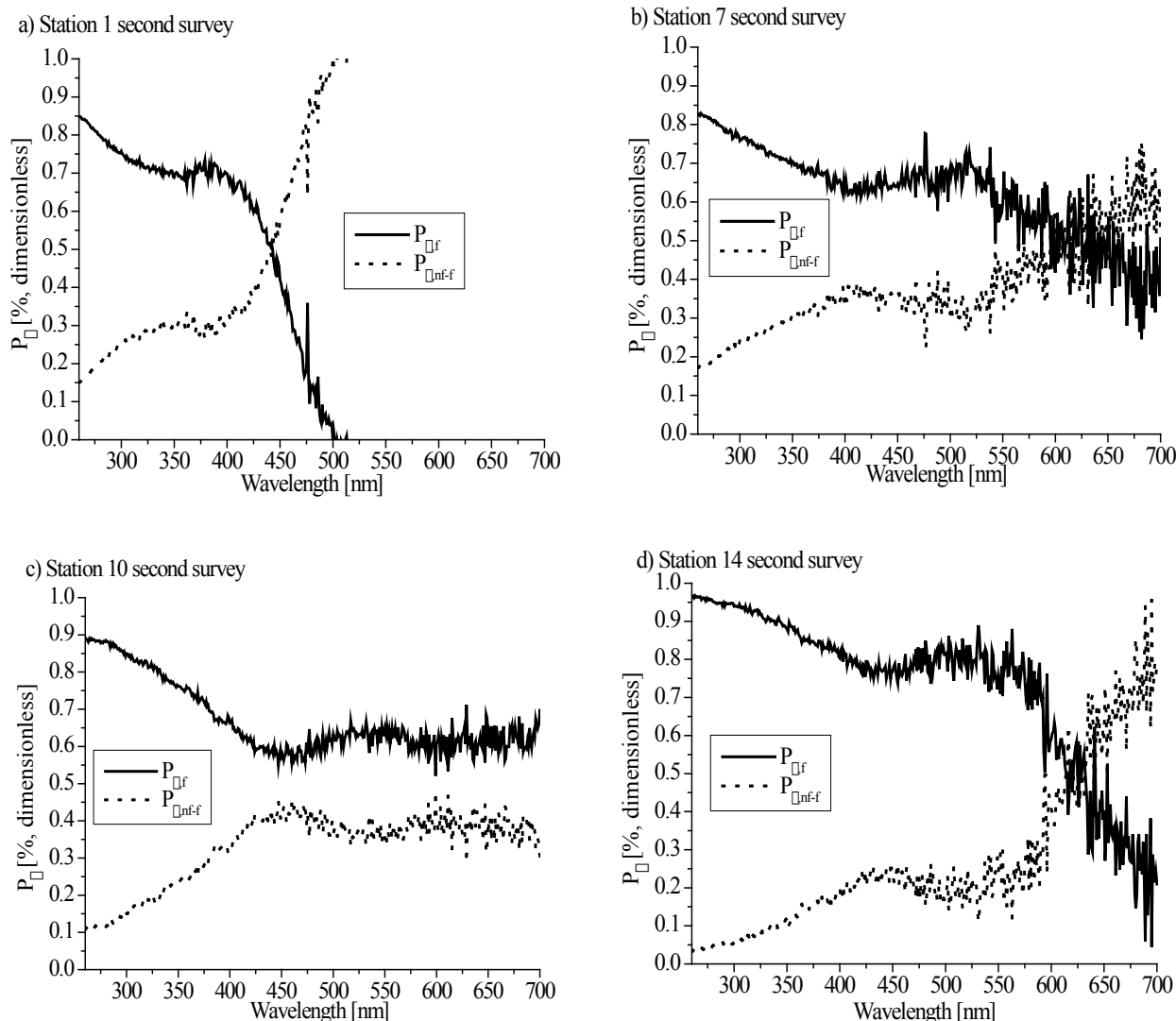


Figure 12: Spectral extinction percentage for the filtered sample extinction (black curve) and  $e_{nf-f}$  computed extinction curve (dot curve) to the total extinction ( $e_{nf}$ ) calculated during the second survey. Panel a station 1, b station 7, c station 10 and panel d station 14.

### 3.4 The spatial distribution of optical and limnological parameters.

A significant and repeatable spatial distribution of 313 nm attenuation coefficient was marked in all the surveys (Figure 14 a, b, c), with the highest attenuation values present in the northern section of the lake.

The spectral slope values (figure 14, d, e, f) were found to be the highest in the southern area of the lake, where the attenuation of the dissolved fraction and the attenuation coefficient at 313 nm were minimal, according therefore with the Del Vecchio and Blough (2002) approach, the southern part of the lake is characterized

by a higher CDOM molecular weight present in lower concentrations. The opposite situation characterizes the northern part of the lake. Different dissolved organic matter sources, having different CDOM initial chemical properties, associated to non linear actions of microbial degradation, direct and indirect photodegradation and photobleaching, contribute all together to create such spatial differences of the spectral slope. The present work is not able to give explanation of the distribution of the spectral slope, but two hypotheses can be made. The first regards the different CDOM sources in the northern and southern part of the lake. In the north, a relative high

quantity of low molecular weight CDOM was probably released, while in the south, it was a relative low quantity of high molecular weight CDOM to be released. A second hypothesis agrees with that of Morris and Hargreaves (1997), which relate diminishing spectral slopes with the CDOM photodegradation process. High slope CDOM released in the northern area diffuses and moves towards the southern basin being affected by photodegradation, induced by increasing doses of irradiance during the transport, the result is low absolute levels of spectral slope in this area.

The spatial distributions of TSS concentrations,  $R_{340}$  and  $I_{nf-f,400-700}$  are presented for the second survey (figure 15 a, b and c). Derived optically properties ( $R_{340}$  and  $I_{nf-f,400-700}$ ) show a spatial relationship with total suspended

particles. For  $R_{340}$  and  $I_{nf-f,400-700}$  positive relationships are founded ( $R^2=0.58$ ,  $N=18$  and  $p<3\times 10^{-4}$ ;  $R^2=0.75$ ,  $N=18$  and  $p<1\times 10^{-4}$  respectively). During the third survey the distribution of CHLa concentrations were replicated by  $R_{340}$  ( $R^2=0.49$ ,  $N=25$ ,  $p<2\times 10^{-4}$ ) and partially by the  $I_{nf-f,400-700}$  ( $R^2=0.45$ ,  $N=19$ ,  $p<0.02$ ) (figure 16 a, b and c). It should be marked that  $I_{nf-f,400-700}$ , calculated from extinction measurements (equation 4), tracks the TSS spatial changes. In both surveys higher values of both, limnological and optically parameters were, found in the north side of the lake. Finally, should be noted the general lower values of the  $R_{340}$  in the second survey (low relative concentration of TSS; figure 15 b) respect the  $R_{340}$  values mapped in the third survey (relative high values of TSS concentrations; figure 16 b).

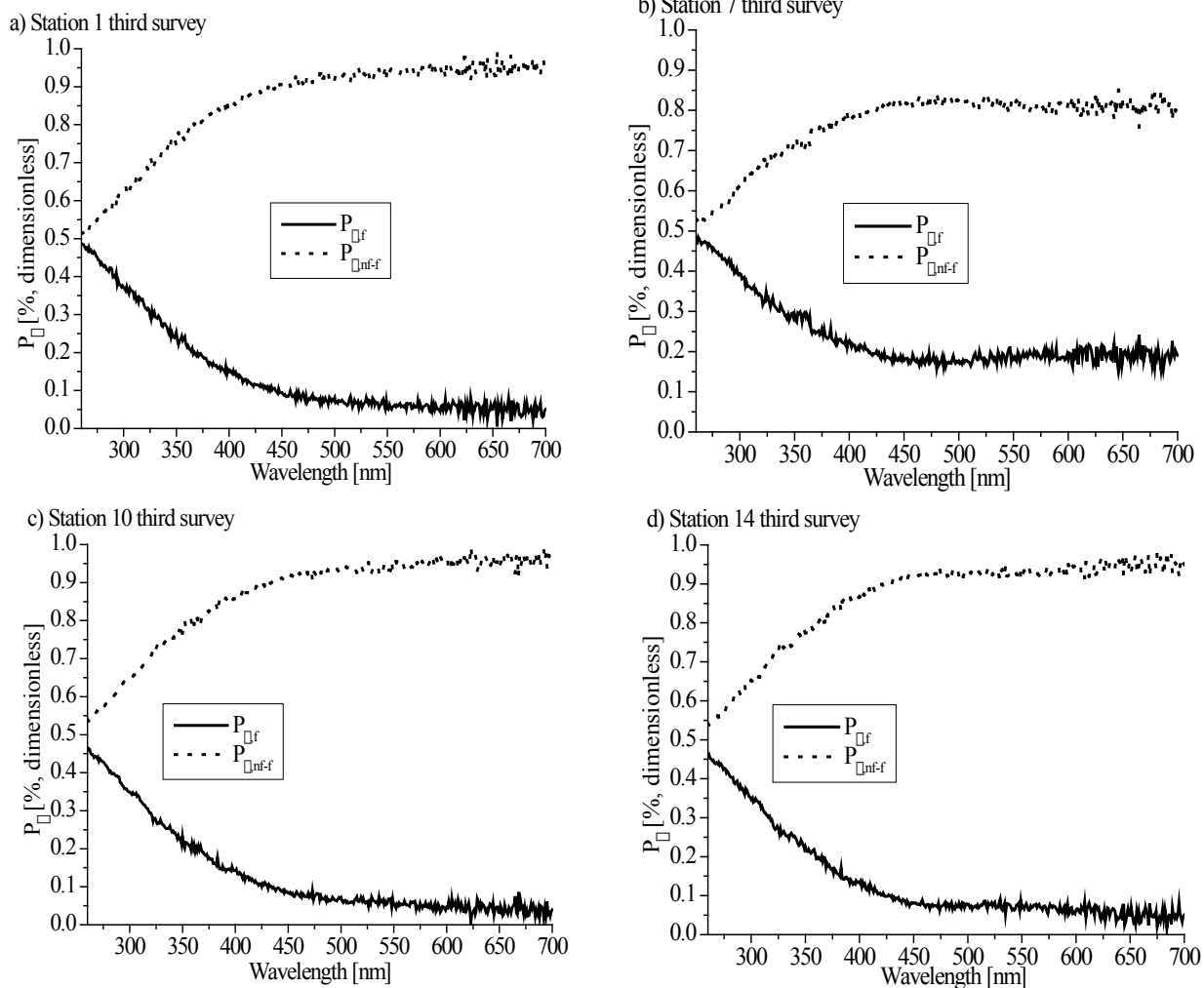


Figure 13: Spectral extinction percentage for the filtered sample extinction (black curve) and  $e_{nf-f}$  computed extinction curve (dot curve) to the total extinction ( $e_{nr}$ ) calculated during the third survey. Panel a station 1, b station 7, c station 10 and panel d station 14.

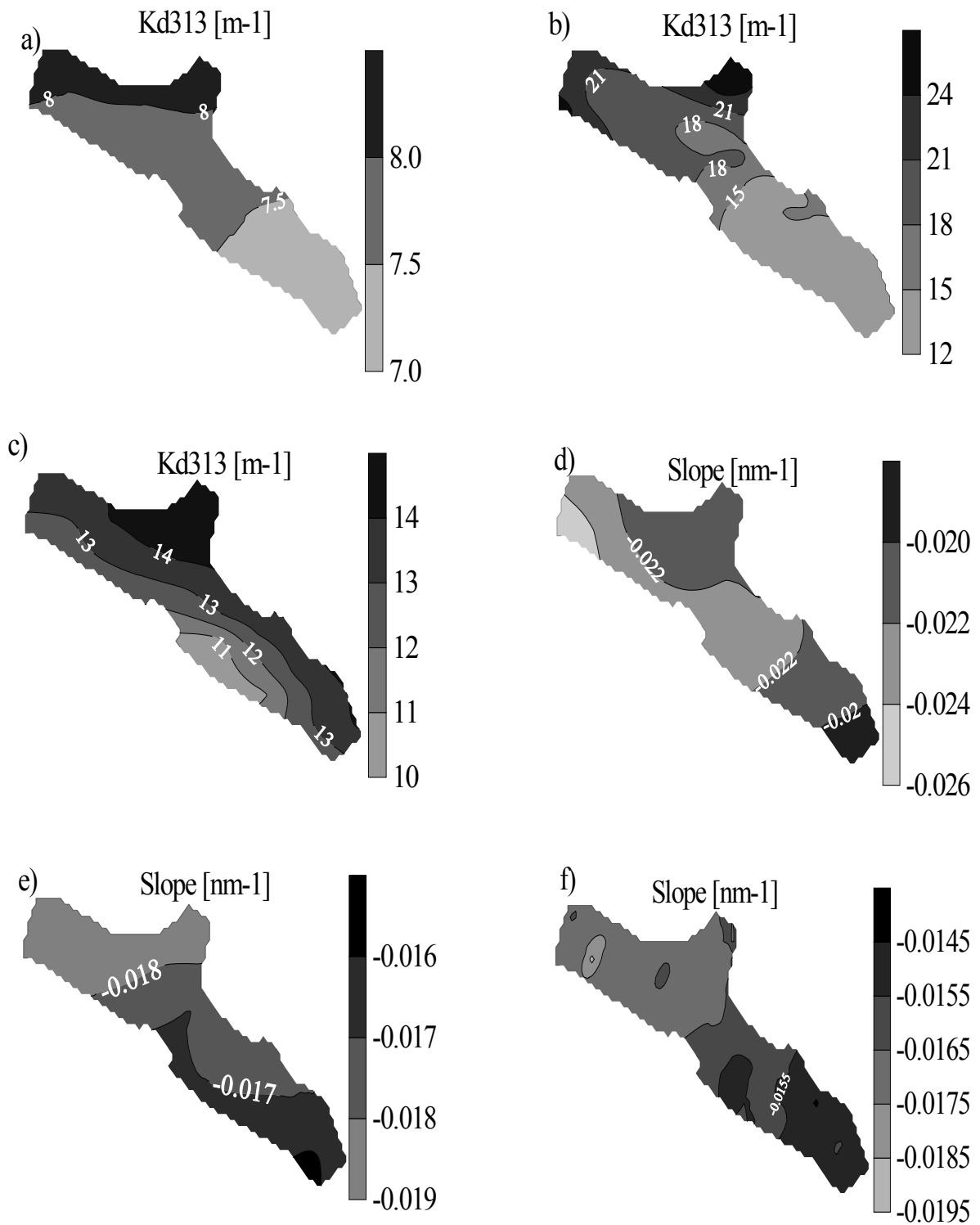


Figure 14: Spatial distribution of the attenuation coefficient at 313 nm during the first (panel a), second (panel b) and last survey (panel c). Spectral slope distribution observed during the first (panel d) second (panel e) and last survey (panel f).

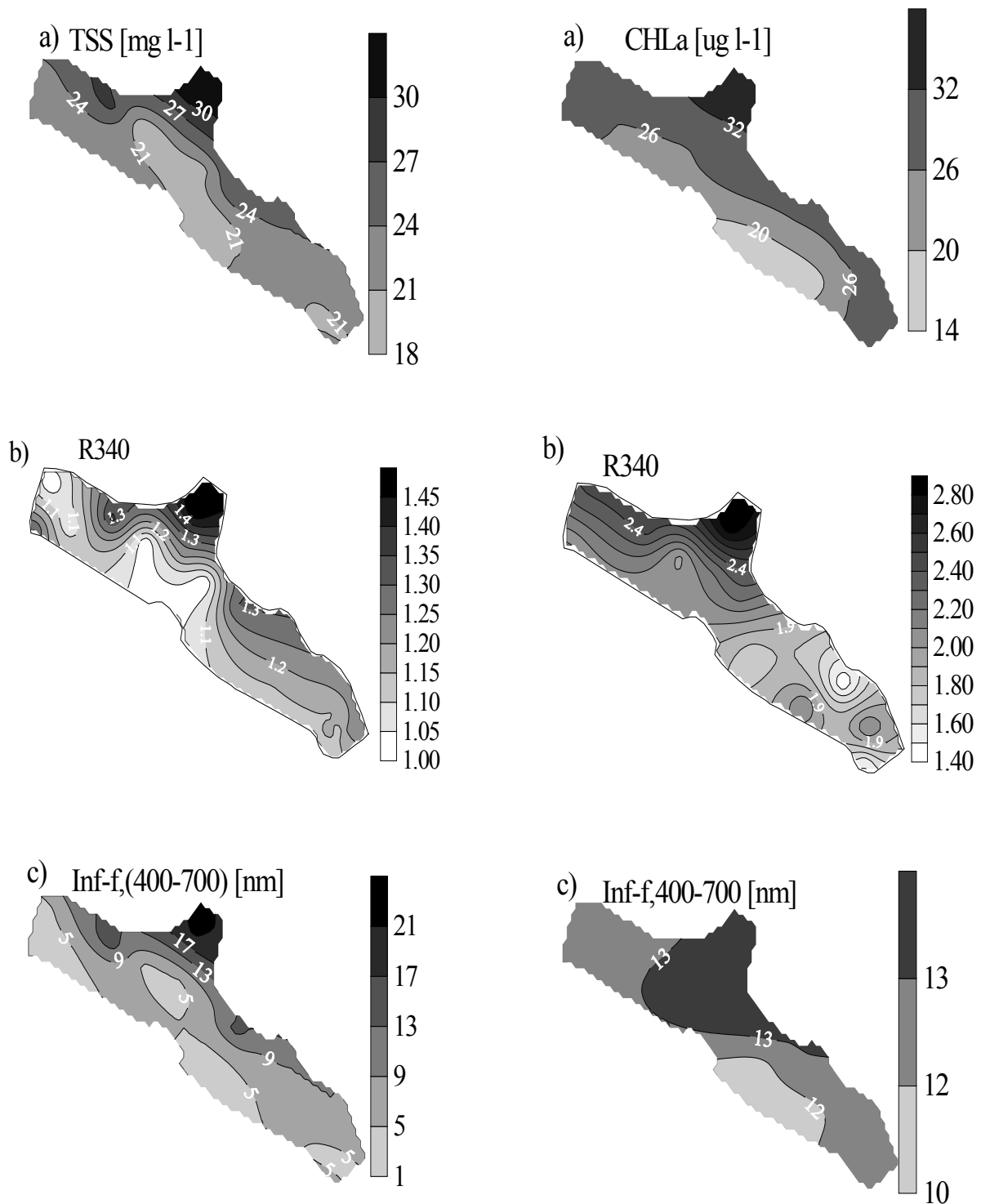


Figure 15: Spatial distribution of the total suspended solid concentrations (TSS),  $R_{340}$  and  $I_{\text{inf-f},400-700}$  during the second survey.

Figure 16: Spatial distribution of the chlorophyll a concentrations (CHLa),  $R_{340}$  and  $I_{\text{inf-f},400-700}$  during the last survey.

## Conclusion

In the present investigation, an optical approach combines in situ attenuation measurements with laboratory extinction determinations. The combination of AOPs and IOPs allows a clear definition of the contribution of each water column fraction to the aquatic natural systems optical properties in time and space. The  $R_\lambda$  ratio and  $I_{\text{nf-f},400-700}$  help to estimate the total suspended solids and its spatial distribution in the aquatic environment. The PAR attenuation coefficient is influenced by relative high concentration of CDOM and by its absorption in the short wavelengths of visible waveband, for this reason the  $R_\lambda$  ratio describes the variations of TSS concentrations more clearly than the  $K_{\text{d,PAR}}$ . The terms  $I_{\text{nf-f},400-700}$  can be assumed as a relative measure of the total suspended solid concentration and  $e_{\lambda,\text{nf-f}}$  is similar to a transmissometer signals without the contribution of the direct light absorption caused by CDOM (formerly cited, (Kirk, 1994; Austin and Petzold, 1977; Bohckov et al., 1980).

Even if the effect of scattering in the spectrophotometer is higher than in situ,

the proposed extinction analysis procedure can be successfully adopted to estimate the distribution of TSS and to obtain information on the role of the suspended and dissolved particles on total extinction. The overall extinction and attenuation of solar radiation in the UV and visible wavelengths is dominated by different components of the water column in relation to meteorological conditions and location. In fact, the wind resuspension led to the increasing of the role of suspended matter in the total attenuation while not modifying the role or concentration of the dissolved matter in the lake.

## Acknowledgements

This work was supported through the Italian University and Research Ministry (MIUR) FIRB programme (RBAU01CM44) and CIRCLE MED "MERCODYN" programme. The Italian Ministry for Agricultural and Forest Policies also supported this research. Authors greatly appreciate the suggestions of two anonymous referees and the help of Dr. Margherita Falcucci, Dr. Luciano Nannicini and Dr. Paolo Riccomi.

## References

- Austin R W, Petzold T J 1977. Considerations in the design and evaluation of oceanographic transmissometers. In: J. E. Tyler (Ed.). *Light in the sea*. Stroudsbury pp 104
- Ayoub L, Hargreaves B R, Morris D P 1997. UVR attenuation in lakes: Relative contribution of dissolved and particulate material., *Ocean Optics XIII, SPIE*, **2963**: 338-352
- Baker K S, Smith R C 1979. Quasi-inherent characteristics of diffuse attenuation coefficient of irradiance, *Ocean Optics VI, SPIE*, **208**: 60-63
- Baker K S, Smith R C 1982. Spectral irradiance penetration in natural water. In J. Calkins (Ed.), *The role of solar ultraviolet radiation in marine ecosystems*, NATO conference series IV, Marine Sciences Plenum Press, New York, pp 233-246
- Belzile C, Vincent WF, Kumagay M 2002. Contribution of absorption and scattering to the attenuation of UV and photosynthetically available radiation in Lake Biwa., *Limnol. Oceanogr.*, **47** ( ) 95-107
- Blumthaler M, Webb A R 2003. UVR climatology. In: Helbling, E.,W., Zagarese, H. (Eds). *UV effects in aquatic organism and ecosystems*. The Royal Society of Chemistry, Cambridge pp575.
- Bochkov BF, Kopelevich OV, Kriman BA 1980. A spectrophotometer for investigating the light of sea water in the visible and ultraviolet regions of the spectrum. *Oceanology*, 20101-104.
- Bracchini L, Cozar A, Dattilo A M, Falcucci M, Gonzales R, Loiselle S, Hull V 2004. Analysis of extinction in ultraviolet and visible spectra of water bodies of the Paraguay and Brazil wetlands, *Chemosphere* **57**: 1245-1255
- Bracchini L, Loiselle SA, Dattilo A M, Mazzuoli S, Cózar A, Rossi C 2004. The spatial distribution of the optical properties in the UV and Visible in an aquatic ecosystem., *Photochem. Photobiol.*, **80**: 139-149.
- Bricaud A, Morel A, Prieur L, 1981. Absorption by dissolved organic matter of the sea (yellow substance) in the UV and visible domains. *Limnol. Oceanogr.* **26**: 43-53
- De Haan H, De Boer T 1987. Applicability of light absorbance and fluorescence as measures of concentration and molecular size of dissolved organic carbon in humic lake Tjeukemeer. *Water Res.*, **21**: 731-734.
- De Haan H 1993. Solar UV light penetration and photodegradation of humic substances in peaty lake water. *Limnol. Oceanogr.*, **38**: 1072-1076.
- Del Vecchio R, Blough N V 2002. Photo-bleaching of chromophoric dissolved organic matter in natural waters: kinetics and modeling. *Mar. Chem.*, **78**: 231-253.
- Gordon HR 1989. Can the Beer-Lambert law be applied to the diffuse attenuation coefficient of oceanic water?, *Limnol. Oceanogr.*, **34**: 1389-1409
- Hargreaves B R 2003. Water column optics and penetration of UVR. In: Helbling, E.,W., Zagarese, H. (Eds). *UV effects in aquatic organism and ecosystems*. The Royal Society of Chemistry, Cambridge pp 575.
- Huovinen P S, Penttila H, Soimasuo M R 2003. **Spectral attenuation of solar ultraviolet radiation in humic lakes in Central Finland.** *Chemosphere* **51**: 205-214.
- Kirk J T O 1981. Monte Carlo study of the nature of the underwater light field in and the relationship between optical properties of turbid yellow waters, *Aust. J. Mar. Freshwater Res.*, **32**: 517-532
- Kirk J T O 1994. Optics of UV-B radiation in natural waters, in: C. E. Williamson and H. E. Zagarese (Eds), *Impact of UV-B radiation on pelagic freshwater ecosystems*, .Schweizerbart, Stuttgart., pp. 1-16
- Kirk J T O 1980. Spectral absorption properties of natural waters: contribution of the soluble and particulate fractions to light absorption in some inland waters of southeastern Australia. *Aust. J. Mar. Freshwater Res.*, **31**: 287-296
- Kirk J T O 1994. *Light & Photosynthesis in Aquatic Ecosystems*, 2<sup>nd</sup> edition. Press Syndicate of the University of Cambridge. Cambridge pp 509
- Laurion I, Vincent W F, Lean D R S 1997. Underwater ultraviolet radiation: development of spectral models for northern high latitude lake, *Photochem. Photobiol.*, **65**: 107-114
- Markager S, Vincent W F 2000. Spectral light attenuation and the absorption of UV and blue light in natural waters. *Limnol. Oceanogr.* **45**: 642-650
- Mobley C D 1994. *Light and water: radiative transfer in Natural waters*. Academic Press, San Diego, Ca, pp 592.
- Morel A 1991. Light and marine photosynthesis: a spectral model with geochemical and climatological implication, *Prog. Oceanogr.*, **26**: 263-306.
- Morel A 1988. Optical Modeling of the Upper Ocean in Relation to Its Biogenous Matter content (Case I Waters), *J. Geophys. Res.* **93**: 10749-10768.
- Morel A, Prieur L 1977. Analysis of variation in ocean colour. *Limnol. Oceanogr.*, **22**: 709-722
- Morris D P, Zagarese H, Williamson C E, Balseiro E G, Hargreaves B R, Modenutti B, Moller R, Queimalinos C 1995. The attenuation of solar UV

- radiation in lakes and the role of dissolved organic carbon. *Limnol. Oceanogr.* **40**:1381-1391.
- Morris D P, Hargreaves B R 1997. The role of photochemical degradation of dissolved organic carbon in regulating the UV transparency of three lakes on the Pocomo Plateau. *Limnol. Oceanogr.* **42**: 239-249
- Prieur L, Sathyendranath S 1981. An optical classification of coastal and oceanic waters based on the specific spectral absorption curves of phytoplankton pigments, dissolved organic matter and other particulate materials, *Limnol. Oceanogr.*, **26**: 671-689
- Scully N M, Lean D R S 1994. The attenuation of ultraviolet radiation in temperate lakes, *Arch. Hydrobiol. Ergebn. Limnol.*, **43**: 135-144
- Shifrin K S 1995. Simple relationships for the Ångström parameter of disperse systems. *Appl. Optics* **34**: 4480-4485.
- Smith R C, Baker K S 1978. Optical classification of natural waters. *Limnol Oceanogr.*, **23**: 260-267.
- Sommaruga R, Psenner R 1997. Ultraviolet radiation in a high mountain lake of the Austrian Alps: Air and underwater measurements., *Photochem. Photobiol.*, **65**: 957-963
- Sommaruga R 2001. The role of solar UV radiation in the ecology of alpine lake, *J. Photochem. Photobiol. B: Biology* **62**: 35-42
- Standard methods, Standard methods for the examination of water and wastewater - 20<sup>th</sup> edition. 1998. Clesceri L.S., Greenberg A.E., and Eaton A.D. (Eds.), American Public Health Association. Washington DC, USA. **2**:57-59.
- Stedmon C. A., Markager S., Kaas H., 2000. Optical properties and signature of chromophoric dissolved organic matter (CDOM) in Danish coastal waters. *Estuar. Coast. Shelf S.* **51**: 267-278
- Strickland J D H, Parsons T R 1972. A Practical Handbook of Seawater Analysis. Fish. Board Can., Bulletin 167 (Second edition).
- Zheng X, Dickey T, Chang G 2002. Variability of the downwelling diffuse attenuation coefficient with consideration of inelastic scattering, *Appl. Opt.*, **41**: 6477-6488